(Preprint) AAS 19-708

DYNAMICS OF A NON-RIGID ORBITAL SIPHON AT A NEAR-EARTH ASTEROID

Andrea Viale*, Colin McInnes* and Matteo Ceriotti*

The orbital siphon is a novel concept for propellantless payload transfer from the surface of a rotating body to orbit. In the context of asteroid mining, the orbital siphon represents an efficient solution to deliver mined material from the asteroid surface to an orbiting station for later processing or storage. The key idea is that the centrifugal-induced force exerted on a tether-connected chain of payload masses assembled from the surface of a rotating body can be large enough to pull the lower masses, to initialize an orbital siphon effect: new payloads are connected to the chain while upper payloads are removed. In this paper, the dynamics of an orbital siphon anchored to two irregularly shaped near-Earth asteroids is investigated, along with the particle dynamics of the material being transport. The siphon is modelled as a closed chain of tether-connected buckets, kept taut by two pulleys, one at the asteroid surface and one attached to an orbiting collecting spacecraft. Buckets are filled with asteroid material, to be delivered to the collecting spacecraft. It is shown that the irregularities of the gravitational field do not introduce instabilities to the orbital siphon system. Without any braking mechanism required, the radial velocity of the siphon does not diverge but reaches a constant value at a steady-state. Moreover, it is shown that the siphon effect is still generated when the anchor moves on the asteroid surface, allowing the mining location to be moved without interrupting the flow of material to the collecting spacecraft.

INTRODUCTION

Exploitation of space resources is one of the key challenges for the future of space exploration. Earth-based observations, as well as recent robotic missions, have shown that near-Earth asteroids could provide a range of useful resources. It has been noted that in some cases these resources are more accessible than lunar resources[1]. Among the available resources are metals (in particular platinum-group metals) and volatiles - such as water. The latter, in particular, would provide consumables and propellant for in-orbit manufacturing, thus revolutionizing space transportation and solar system exploration[2].

A range of studies have been devoted to the analysis of asteroid mining scenarios. However, the problem of gathering material from the surface for later processing is still largely unexplored. Some authors envision the direct launch of material from the asteroid surface into orbit or for material sorting[3,4]. However, this requires external work to be done in launching the asteroid material. Moreover, this scenario is affected by uncertainties when launching material from the surface for example for repeatability of mass driver launches.

In this paper, a propellantless self-sustaining structure to deliver material from the asteroid surface to an orbiting collecting spacecraft (CS) is considered. The structure physically connects a point on the asteroid surface to the CS, thus avoiding any targeting issues. At the core of the concept, the so-called *orbital siphon* (originally devised by Davis[5,6]), is a chain of tethered-connected payloads, long enough such that the overall centripetal pull due to the asteroid rotation overcomes the gravitational force acting on each payload. This allows the entire chain to lift payloads into orbit: such an *orbital siphon effect* can be exploited to deliver a continuous mass flow of material from the surface of the asteroid the CS.

The authors have previously studied the dynamics of the system under different sets of assumptions and approximations. In Reference 7 the siphon dynamics is studied assuming that the chain of masses can slide

*James Watt School of Engineering, University of Glasgow (UK).

on a rigid support anchored to the equator of a spherical asteroid. This avoids any rotation of the chain generated by inertial forces. Under these simplifying hypotheses the dynamics can be studied analytically. In particular, it was shown that the asteroid mass reduction lowers the siphon effect over time, until the siphon can no longer lift material after a certain fraction of asteroid has been removed. It has been shown that, for a siphon with constant length and an asteroid initially rotating at its critical angular velocity (i.e., at a spin rate at which the centrifugal-induced acceleration at the asteroid equator equals in magnitude the gravitational acceleration thus allowing a particle at the equator to lift off) about 12% of the initial asteroid mass can be disassembled.

In Reference 8 it was proposed that the payload masses could slide on a tether acting as a support structure, similarly to the space elevator concept but with multiple tether-connected payloads instead of a single payload. The chain of payloads would then lift thanks to the orbital siphon effect. A ballast mass at the top of the support tether can be used to reduce the equatorial oscillations of the system, induced by the inertial Coriolis forces.

The dynamics of an orbital siphon anchored to an ellipsoidal asteroid is currently under development. Modelling the asteroid as an ellipsoid allows analysis of the siphon dynamics by varying the ellipsoid shape. It is proposed to exploit the stable equilibrium points associated with the effective potential of a rotating ellipsoid as gravitational depots to store material lifted with the orbital siphon. It is shown the the energy requirement to move material form the surface of the asteroid to an equilibrium point exploiting the orbital siphon dynamics is smaller than launching material from the surface, using for example a mass driver device.

In this paper, the hypothesis of a rigid structure supporting the sliding payload masses is removed and the siphon is modelled as a n-body closed chain of buckets, kept in tension by two pulleys, one at the surface of the asteroid and one attached to an orbiting collecting spacecraft (CS). Buckets are filled with asteroid material, which will be termed the *payload*. When a bucket reaches the upper pulley at the CS, the payload is released to the CS while the bucket will then descend towards the anchor pulley. Similar to a bucket-conveyor, the chain of buckets continuously cycles, due to the siphon effect generated on the lifting side of the chain. Moreover, the gravity environment of the asteroid is simulated using three dimensional triangular-faced polyhedron shape models of near-Earth asteroids 101955 Bennu and 6489 Golevka.

The paper is structured as follows. The dynamical system, the asteroid gravitational environment and the assumptions are firstly introduced. Then, results under different scenarios are presented, by varying siphon parameters and the asteroid properties. Siphons with a moving base are also analysed. Finally, practical aspects related to the siphon deployment and operation are discussed. In particular, preliminary results on the granular dynamics of payload material inside the buckets and during release are provided.

SYSTEM DESCRIPTION, ASSUMPTIONS AND DYNAMICAL MODEL

The key idea behind the orbital siphon concept is that a chain of tethered connected payload masses arranged from the surface of a rotating asteroid experiences a net radial force which can be exploited to raise the entire chain without any external force needed. Then, an orbital siphon effect can be established if new payloads are added at the bottom of the chain and the upper payloads are released. Upper payloads can be released to a bound orbit around the asteroid, to escape or to an orbiting station.

In the scenario presented in this paper payloads are released at an orbiting CS (see Fig. 1). The chain of masses is designed similarly to a bucket conveyor, with consecutive buckets connected to neighbouring buckets via massless elastic tethers with axial Young modulus E, constant cross section A, viscosity coefficient C and unstrained length l. Buckets on the *lifting side* (LS) are filled with payload masses m_p, i.e., raw material mined from the asteroid. The *descending side* (DS) of the siphon hosts empty buckets, returning to the asteroid surface for refilling, after having released their payload mass to the CS, which is physically connected to the siphon through a pulley. Another pulley at the anchor ensures continuous cycling of the buckets.

It is assumed that the pulley size is much smaller than the chain length and therefore the pulleys are modelled as point masses. This choice offers significant savings in computational time with respect to a finite-size pulley. In fact, a finite-size pulley would require modelling the tether with intermediate nodes,

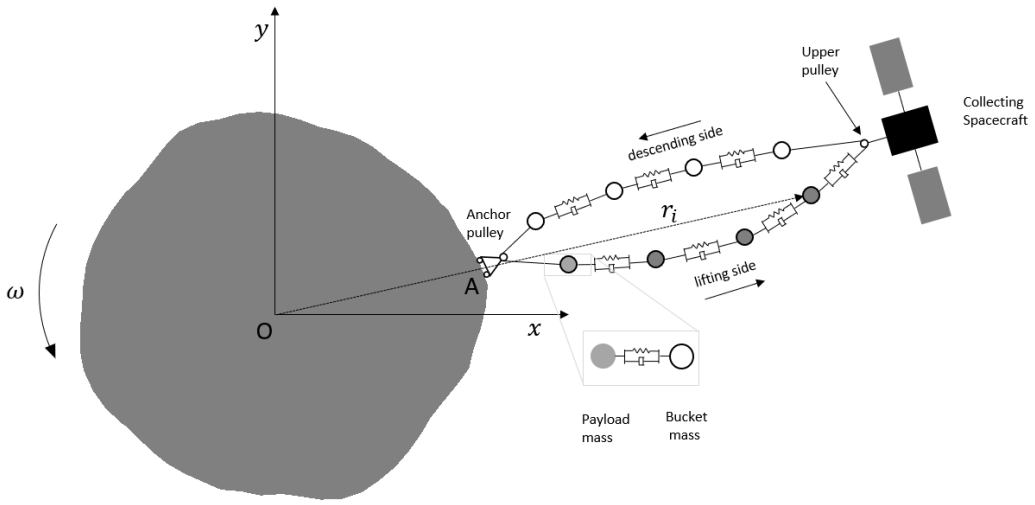

Figure 1: Dynamical model of an orbital siphon anchored to a rotating asteroid. For the sake of clarity the siphon is represented on the asteroid xy plane.

separated by a distance smaller then the diameter of the pulley itself, thus considerably increasing the number of degrees of freedom of the system and the computational time. Any friction between the tether and the pulley is here neglected.

When a bucket reaches the anchor pulley, it is refilled with a new payload. In References 7 and 8 this event was modelled as an inelastic impact, resulting in a discontinuous velocity variation of the system (note that the "waiting" payload is at rest with respect to the siphon, in the asteroid reference frame). This choice may cause numerical instabilities in this model. Hence, the bucket refilling is modelled using a spring-dashpot connection between the bucket and the new payload. Then, the first bucket mass on the LS and the corresponding payload mass are considered as separate point masses, with position vectors $\mathbf{r}_1$ and $\mathbf{r}_{p1}$ respectively, connected via a spring with stiffness k and damping constant c. Once the bucket reaches a sufficient altitude, the payload is then fixed to the bucket. Here, it is chosen to fix the payload to the bucket when another bucket reaches the anchor. For all the other buckets on the LS, the mass of the payloads is simply summed to that of the bucket, without considering two separate masses.

It is assumed that the size of the CS is much smaller with respect to the distance L between the anchor and the CS center-of-mass. For this reason, the CS is also modelled as a point mass, located in the same position as the upper pulley. Although this choice does not allow a model of the CS attitude, this approximation permits the effect of the CS mass variation (increasing over time, as more payload masses are released) to be included into the siphon dynamics.

Let xyz be an asteroid-fixed reference frame centered on the asteroid center-of-mass, with the z axis aligned with the axis of maximum inertia of the asteroid. Then, let $\mathbf{r}_i$ be the position vector from the origin to the i-th bucket of the chain. The equation of motion of the i-th bucket is then

$$\ddot{\mathbf{r}}_i + 2\boldsymbol{\omega} \times \dot{\mathbf{r}}_i + \boldsymbol{\omega} \times (\boldsymbol{\omega} \times \mathbf{r}_i) = \nabla U(\mathbf{r}_i) + \mathbf{F}^i_{tether}/m_i \tag{1}$$

where $\boldsymbol{\omega}$ is the angular velocity of the asteroid, U is the gravitational potential of the asteroid and $\mathbf{F}^i_{tether}$ is the total force generated by the two tethers connected to the i-th bucket. The term m_i is the mass of the buckets, including the payload mass if the bucket is travelling on the LS.

The potential U can be modified to include the centrifugal potential:

$$V(\mathbf{r}_i) = \frac{1}{2}(\boldsymbol{\omega} \times \mathbf{r}_i) \cdot (\boldsymbol{\omega} \times \mathbf{r}_i) + U(\mathbf{r}_i) \tag{2}$$

such that the equations of motion reduce to

$$\ddot{\mathbf{r}}_i + 2\boldsymbol{\omega} \times \dot{\mathbf{r}}_i = \nabla V(\mathbf{r}_i) + \mathbf{F}^i_{tether} \tag{3}$$

By extension, the equations of motion of the entire dynamical system, including the CS and the payload mass m_{p1} attached to the bucket closest to the anchor are

$$\ddot{\mathbf{r}}_i + 2\boldsymbol{\omega} \times \dot{\mathbf{r}}_i = \nabla V(\mathbf{r}_i) + \mathbf{F}^i_{tether}/m_i \tag{4a}$$

$$\ddot{\mathbf{r}}_{cs} + 2\boldsymbol{\omega} \times \dot{\mathbf{r}}_{cs} = \nabla V(\mathbf{r}_i) + \mathbf{F}^{cs}_{tether}/m_{cs} \tag{4b}$$

$$\ddot{\mathbf{r}}_{p1} + 2\boldsymbol{\omega} \times \dot{\mathbf{r}}_{p1} = \nabla V(\mathbf{r}_{p1}) + \mathbf{F}^{p1}/m_p \tag{4c}$$

where $\mathbf{r}_{cs}$ is the position vector of the CS, $\mathbf{F}^{cs}_{tether}$ represents the tether forces acting on the CS, $\mathbf{F}^{p1}$ includes the contact forces used to model the interaction between the new payload mass attached to the chain and the first bucket mass on the LS. Note that for the bucket closest to the anchor pulley, $\mathbf{F}^i_{tether}$ includes the force $-\mathbf{F}^{p1}$ due to the interaction between the bucket and the payload.

Equations 4 can be reduced to a form suitable for numerical integration:

$$\dot{\xi} = A\xi \tag{5}$$

where $\xi = \{u, \dot{u}\}$, and u is a vector containing the coordinates of the buckets, the CS and the first payload mass:

$$u = \{x_1, y_1, z_1, \ldots, x_n, y_n, z_n, x_{cs}, y_{cs}, z_{cs}, x_{p1}, y_{p1}, z_{p1}\}^T \tag{6}$$

The matrix A contains time-dependent terms due to inertial forces, gravitational forces and tension forces. Equation 5 can be numerically integrated in a given time range for a given initial state ξ_0. Integration is interrupted when a bucket reaches a pulley, to modify the direction of the velocity of the bucket intersecting the pulley. In particular, the following two cases are considered:

1. A bucket reaches the CS pulley. The payload mass m_p contained within the bucket is summed to the CS mass. The direction of the velocity of the bucket is then changed such that it is parallel to the vector connecting the CS with the first bucket on the DS closest to the CS. The velocity magnitude is not changed.

2. A bucket reaches the anchor pulley. Let i_0 be the index of this bucket. A payload mass m_p is connected to the i_0-th bucket via a spring-dashpot connection characterized by stiffness k and damping constant c. The direction of the velocity of the i_0-th bucket is then changed such that it is parallel to the vector connecting the anchor with the first bucket on the LS closest to the anchor. The velocity magnitude of the bucket is not changed. The spring-dashpot connection between the $(i_0 + 1)$-th bucket and the corresponding payload is removed, by fixing the payload to the bucket.

In the next sections the equations governing the gravitational potential and the tether forces are presented.

Asteroid gravitational environment

The asteroid is now modelled as a constant and uniform density triangular-faced polyhedron. This choice permits the model to resolve surface irregularities of an asteroid (e.g., cavities, craters or overhangs) and hence study the behaviour of the orbital siphon in a general, non-spherical gravity field.

The polyhedron is defined by the coordinates of its vertexes and the connection topology, describing how the vertexes are connected with respect to each other. Werner and Scheeres[9] showed how the gravitational potential around a constant density polyhedron and its gradient can be reduced to a summation over its edges

and faces:

$$U(\mathbf{r}) = \frac{G\rho}{2}\left[\sum_{e\in\text{edges}} \mathbf{r}_e \cdot \mathbf{E}_e \cdot \mathbf{r}_e L_e - \sum_{f\in\text{faces}} \mathbf{r}_f \cdot \mathbf{F}_f \cdot \mathbf{r}_f \gamma_f\right] \tag{7}$$

$$\nabla U(\mathbf{r}) = -G\rho\left[\sum_{e\in\text{edges}} \mathbf{E}_e \cdot \mathbf{r}_e L_e - \sum_{f\in\text{faces}} \mathbf{F}_f \cdot \mathbf{r}_f \gamma_f\right] \tag{8}$$

where $G = 6.674\,28 \times 10^{-11}\,\mathrm{m^3\,kg^{-1}\,s^{-2}}$ is the gravitational constant, ρ is the density of the asteroid, $\mathbf{r}_e$ ($\mathbf{r}_f$) is a body fixed vector from any point on the edge (face) to the field point considered and the other parameters are defined in terms of the face geometry and orientation. $\mathbf{E}_e$ and $\mathbf{F}_e$ are second order tensors depending on the properties of the edges and the faces, L_e is a quantity proportional to the length of each edge whereas γ_f is the solid angle associated with each face, as seen from the field point. For a triangular-faced polyhedron:

$$\mathbf{E}_e = \hat{\mathbf{n}}_f \hat{\mathbf{n}}_e^f + \hat{\mathbf{n}}_{f'} \hat{\mathbf{n}}_e^{f'} \tag{9}$$

$$\mathbf{F}_f = \hat{\mathbf{n}}_f \hat{\mathbf{n}}_f \tag{10}$$

$$L_e = \ln \frac{r_1^e + r_2^2 + e_e}{r_1^e + r_2^e - e_e} \tag{11}$$

$$\gamma_f = 2\tan^{-1} \frac{\mathbf{r}_1^f \cdot \mathbf{r}_2^f \cdot \mathbf{r}_3^f}{r_1^f r_2^f r_3^f + r_1^f \mathbf{r}_2^f \cdot \mathbf{r}_3^f + r_2^f \mathbf{r}_3^f \cdot \mathbf{r}_1^f + r_3^f \mathbf{r}_1^f \cdot \mathbf{r}_2^f} \tag{12}$$

where $\mathbf{r}_j^f, (j = 1, 2, 3)$ are the position vectors of face vertexes, taken in counter-clockwise order about the normal to the face, $\hat{\mathbf{n}}_f$, $\mathbf{r}_j^e, (j = 1, 2)$ are the two position vectors of the edge, $\hat{\mathbf{n}}_e^f$ is a unit vector normal to the edge and to the corresponding face normal $\hat{\mathbf{n}}_f$, e_e is the length of the edge.

Tether tension forces

Let $\mathbf{q}_j$ be the relative displacement between the j-th and $(j+1)$-th mass of the chain, so that

$$\mathbf{q}_j = (x_{j+1} - x_j)\hat{\mathbf{i}} + (y_{j+1} - y_j)\hat{\mathbf{j}} + (z_{j+1} - z_j)\hat{\mathbf{k}}. \tag{13}$$

Here $\hat{\mathbf{i}}$, $\hat{\mathbf{j}}$ and $\hat{\mathbf{k}}$ are the unit vectors parallel to the x, y and z directions. Then, the tension forces acting on the j-th mass are modelled according to Hooke's law, and therefore depend on the displacements $\mathbf{q}_j$ and $\mathbf{q}_{j-1}$:

$$\mathbf{F}_j^s = EA\epsilon_j \frac{\mathbf{q}_j}{|\mathbf{q}_j|} - EA\epsilon_{j-1} \frac{\mathbf{q}_{j-1}}{|\mathbf{q}_{j-1}|}. \tag{14}$$

Here, ϵ_j is the strain of the j-th tether, given by

$$\epsilon_j = \begin{cases} \dfrac{(|\mathbf{q}_j| - l)}{l} & \text{if} \quad |\mathbf{q}_j| > l \\ 0 & \text{if} \quad |\mathbf{q}_j| \leq l \end{cases} \tag{15}$$

Note that the tether cannot support axial compressions, thus the tension vanishes when the tether becomes slack.

If the j-th tether is in contact with one of the two pulleys, let $\mathbf{q}_i^a = \mathbf{r}_P - \mathbf{r}_i$ be the relative displacement between the j-th mass and the pulley, where $\mathbf{r}_P = \{x_P, y_P, z_P\}$ is the position vector of the pulley and $\mathbf{q}_j^b = \mathbf{r}_{j+1} - \mathbf{r}_P$ is the relative displacement between the pulley and the $(i+1)$-th mass. It is assumed that the tension on the j-th tether is constant between the two sections $\mathbf{q}_j^a$ and $\mathbf{q}_j^b$. Note that this is an approximation, as the pulley normally alters the tensions on the tether if friction at the tether-pulley interface is considered. Therefore, the assumption of a constant tension of the tether intersecting the pulley node is equivalent to assuming that the tether is sliding over the pulley. In this case the strain along the tether is given by

$$\epsilon_j = \frac{|\mathbf{q}_j^a| + |\mathbf{q}_j^b| - l}{l} \tag{16}$$

Tether damping forces

It is assumed that the damping forces are proportional to the strain rate $\dot{\epsilon}_j$. From Eq.(15) it can be shown that:

$$\dot{\epsilon}_j = \begin{cases} \dfrac{\dot{\mathbf{q}}_j \cdot \mathbf{q}_j}{|\mathbf{q}_j| l} & \text{if} \quad |\mathbf{q}_j| > l \\ 0 & \text{if} \quad |\mathbf{q}_j| < l \end{cases} \tag{17}$$

where

$$\dot{\mathbf{q}}_j = (\dot{x}_{j+1} - \dot{x}_j)\hat{\mathbf{i}} + (\dot{y}_{j+1} - \dot{y}_j)\hat{\mathbf{j}} + (\dot{z}_{j+1} - \dot{z}_j)\hat{\mathbf{k}} \tag{18}$$

Then, the total damping force contribution to the motion of the j-th mass is given by

$$\mathbf{F}_j^d = C\dot{\epsilon}_j \frac{\mathbf{q}_j}{|\mathbf{q}_j|} - C\dot{\epsilon}_{j-1} \frac{\mathbf{q}_{j-1}}{|\mathbf{q}_{j-1}|} \tag{19}$$

If the j-th tether is in contact with one of the two pulleys, the strain rate is obtained by taking the time derivative of Eq. (16), under the assumption that the damping force remains constant over the tether crossing the pulley:

$$\dot{\epsilon_j} = \frac{1}{l}\left[\frac{\mathbf{q}_j^a \cdot \dot{\mathbf{q}}_j^a}{|\mathbf{q}_j^a|} + \frac{\mathbf{q}_j^b \cdot \dot{\mathbf{q}}_j^b}{|\mathbf{q}_j^b|}\right] \tag{20}$$

Then, the total tether force acting on the j-th mass is the sum given by

$$\mathbf{F}_{tether}^j = \mathbf{F}_j^s + \mathbf{F}_j^d \tag{21}$$

Tether forces on the collecting spacecraft

The dynamics of the CS is governed by Eq. (4b). Using the notation introduced above, the force $\mathbf{F}_{tether}^{CS}$ acting on the CS is written as

$$\mathbf{F}_{tether}^{CS} = (EA\epsilon_j + C\dot{\epsilon}_j)\frac{\mathbf{q}_j^b}{|\mathbf{q}_j^b|} - (EA\epsilon_j + C\dot{\epsilon}_j)\frac{\mathbf{q}_j^a}{|\mathbf{q}_j^a|} \tag{22}$$

where the index j in this case refers to the tether in contact with the pulley. Note that any other external force generated by the contact between the released material and the CS is here neglected.

Orbital siphon effect

In order to generate the orbital siphon effect, the centrifugal-induced force on the uppermost buckets of the siphon has to be large enough to pull the lowermost buckets of the chain, the lowermost buckets being characterized by a larger gravitational attraction towards the asteroid. Clearly, the longer the chain, the larger the centrifugal-induced force on the uppermost buckets.

Figure 2 shows the sum of the gravitational and centrifugal-induced force per unit mass on the LS of the siphon (assuming that all the buckets and payloads have the same mass, the dimensional force is obtained by multiplying this value by the overall mass on the LS), when the anchor longitude is varied in the range $[0, 2\pi]$ and the anchor latitude is zero, for different chain lengths and number of payload masses, for the asteroid Bennu and Golevka (see Table 1 for physical properties). Here, the contribution of the DS is not considered (the buckets on the DS would generate a force which is transmitted to the LS via the tether intersecting the anchor pulley, thus slightly decreasing the net force). The chain of masses is assumed to be parallel to the vector OA (see Fig. 1) for the given anchor longitude. Note that, in general, this force will be a three-dimensional vector with non-zero values on each component (due to the irregularity of the gravitational field). The value shown here is the projection of the force per unit mass onto the direction parallel to the vector OA. If this force is negative, it is expected that the siphon will fall onto the surface, so that a positive force is required. Note that it is not possible to predict *a priori* whether the siphon will keep the same radial

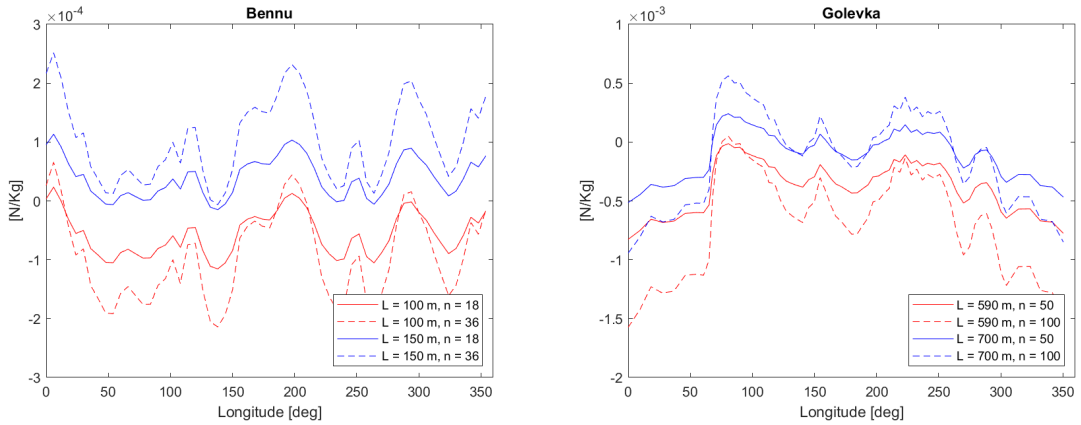

(a) (b)

Figure 2: Force per unit LS mass acting on a siphon anchored at different equatorial longitudes on the asteroid Bennu (2a) and Golevka (2b), for different siphon lengths (L) and number of buckets n.

Period[10,11]	$4.297\,\mathrm{h}$	$6.0289\,\mathrm{h}$
Density[10,12]	$1.26\,\mathrm{g\,cm^{-3}}$	$2.7\,\mathrm{g\,cm^{-3}}$
Equivalent sphere radius	$246\,\mathrm{m}$	$265\,\mathrm{m}$
Polyhedron vertexes	1348	2048
Polyhedron faces	2692	4092

Table 1: Physical properties of Bennu and Golevka and polyhedra details. Shape models are taken from Reference 13 and 11 respectively.

orientation during the simulation (this issue will be addressed in the next sections). Here, the analysis is simplified by considering the statics of a chain parallel to OA to show how the siphon length and anchor longitude influence the force on the siphon. For an ideal spherical asteroid, the force represented here would be constant.

As expected, longer chains are associated to larger forces. For example, a $100\,\mathrm{m}$ chain anchored on Bennu with 18 payload masses on the LS is subjected to a positive force if the siphon is anchored near longitude $0\,\mathrm{deg}$ or $200\,\mathrm{deg}$. By increasing the length, other longitudes can be used to anchor the siphon. For example, by taking a $150\,\mathrm{m}$ chain, almost any equatorial location around Bennu generates an orbital siphon effect. It is interesting to note that increasing the number of elements on the chain does not necessarily increase the force on the siphon.

The results for Golevka (Fig. 2b) are similar, even though the chain length to generate the orbital siphon effect are much larger than the case of Bennu. In fact, although the average radius of Bennu and Golevka are comparable, the density of Golevka is larger than the density of Bennu, and Golevka is spinning with a lower angular velocity.

SIMULATED CASE STUDIES

Simulations are now performed considering the two near-Earth asteroids 101955 Bennu and 6489 Golevka. Physical properties and details of the polyhedral models used are given in Table 1. Figure 3 shows the shape models of the two asteroids. Bennu has a spinning top-shape and a ridge along the equatorial region. Bennu is the 4-th most profitable known asteroid for mining purposes * within the near-Earth asteroid population.

*According to *asterank.com*

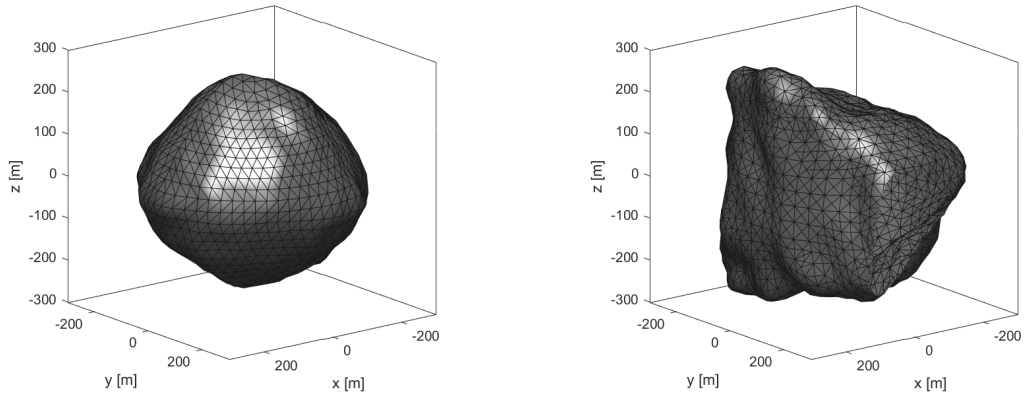

(a) (b)

Figure 3: Shape models for Bennu (3a) and Golevka (3b).

Golevka has a more irregular shape and hence it represents an interesting case study for the orbital siphon, to understand how the gravitational field influences the siphon dynamics.

It is assumed that both asteroid are principal axis rotators[10, 14], i.e., their angular velocity vector is aligned with their maximum moment of inertia axis (here the z axis) and therefore maintain a constant angular velocity in absence of external torques. Precession and nutation are neglected as the large majority of asteroids in a complex rotational state are characterized by a slow rotational rate (unlike Bennu and Golevka) and therefore are not suitable for this application. A slow rotation rate would be associated with very large orbital siphon structures.

Figure 4 shows the magnitude of the effective acceleration on the surface of the two asteroids. For a given point $\mathbf{r}$ on the surface, this is the norm of the vector $\nabla V(\mathbf{r})$, where V the effective potential defined by Eq. (2). In the case of the asteroid Bennu, the effective acceleration is larger at the poles and lower at the equatorial region (this trend is typical for spheroidal asteroids). In fact, close to the poles, the centrifugal-induced acceleration is small and thus the gradient of the effective potential V is mainly influenced by the gravitational field. Moving away from the poles, the centrifugal-induced acceleration increases, thus competing with the gravitational acceleration and reducing $|\nabla V(\mathbf{r})|$. Although not directly represented here, the vector ∇V points inward across the surface of the asteroid.

The map of $|\nabla V(\mathbf{r})|$ does not follow the same pattern on the surface of the asteroid Golevka, due to its more irregular shape. The acceleration is minimized in a region close to the y-axis (green axis) and is larger at the polar regions and in proximity of the x-axis, where there is a large plateau close to the rotation axis.

In order to minimize the siphon length for a given radial force, the siphon should be located in a region where $|\nabla V(\mathbf{r})|$ is small, i.e., where the centrifugal-induced acceleration is larger than the gravitational acceleration.

The following scenarios are analysed:

1. Bennu: orbital siphon with a fixed anchor. The simulations are performed for three cases, varying the siphon length and/or payload mass

   (a) $m_p = 34\,\mathrm{kg}$, $L = 97\,\mathrm{m}$,

   (b) $m_p = 126\,\mathrm{kg}$, $L = 97\,\mathrm{m}$,

   (c) $m_p = 34\,\mathrm{kg}$, $L = 120\,\mathrm{m}$.

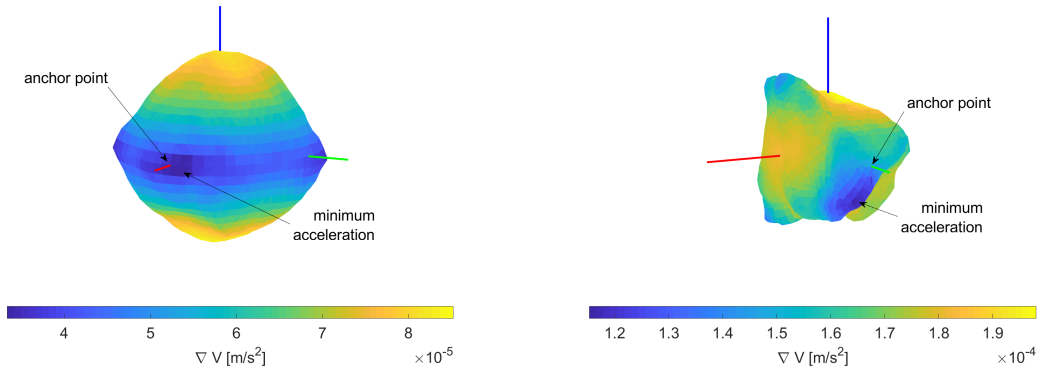

(a) (b)

Figure 4: Surface acceleration for Bennu (4a) and Golevka (4b). The red, green and blue line represent the x, y and z axis respectively.

The two different payload masses correspond to the mass of asteroid material which can be filled in a cubic bucket with size $30\,\mathrm{cm}$ or $46\,\mathrm{cm}$ (neglecting material porosity). The bucket mass is calculated assuming the bucket is made of Aluminium 7075-T6 with a density of $2.81\,\mathrm{g\,cm^{-3}}$ and each face has a thickness of $1\,\mathrm{mm}$. This leads to $m_b = 1.5\,\mathrm{kg}$ for the smaller bucket and $m_b = 3.5\,\mathrm{kg}$ for the larger bucket. The orbital siphon is anchored to the point $\{285.6, 00\}$, which is the intersection between the x-axis and the asteroid surface (see Fig 4a). In all cases the initial mass of the CS is assumed to be $800\,\mathrm{kg}$.

2. Golevka: orbital siphon with a fixed anchor. A $590\,\mathrm{m}$ chain with 105 payloads is used for the simulation. The siphon is anchored to the point $\{0, 342.94, 0\}$, which is the intersection between the y-axis and the asteroid surface (Fig. 4b). A $30\,\mathrm{cm}$ side cube is used for this simulation, corresponding to a payload mass $m_p = 73\,\mathrm{kg}$ (note that in this case more mass can be filled in the $30\,\mathrm{cm}$ bucket due to the larger density of Golevka). In this case two scenarios are studied, to analyze the effect of the CS mass at the beginning of the mass transfer process:

   (a) $m_{cs}(t = 0) = 1600\,\mathrm{kg}$,

   (b) $m_{cs}(t = 0) = 2400\,\mathrm{kg}$.

3. Bennu: orbital siphon with moving base. The siphon base undergoes a constant velocity motion on the asteroid surface for example, to move to a new mining location without interrupting the flow of material. The initial base point is the same as Scenario 1 and two cases are here considered:

   (a) Longitudinal motion of the anchor base, with siphon length $97\,\mathrm{m}$. The anchor is moved by $60\,\mathrm{m}$ towards the positive y direction, with constant anchor velocity $1 \times 10^{-3}\,\mathrm{m\,s^{-1}}$.

   (b) Latitudinal motion of the anchor base, with siphon length $120\,\mathrm{m}$. The anchor is moved by $30\,\mathrm{m}$ towards the positive z direction, with constant anchor velocity $1 \times 10^{-3}\,\mathrm{m\,s^{-1}}$.

   Note that the chain is larger in the second case. This is to generate the siphon effect when the anchor moves towards larger latitudes and $|\nabla V|$ increases on the surface (Fig. 4a). In both cases the payload mass is $34\,\mathrm{kg}$ and the initial mass of the CS is $800\,\mathrm{kg}$.

The selected anchor locations for scenarios 1 and 2 are close to the region of minimum effective acceleration, where the relative magnitude of the centrifugal-induced acceleration is larger. (see Fig. 4).

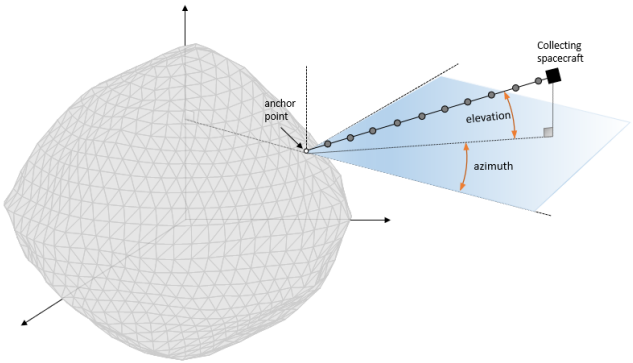

Figure 5: Definition of azimuth and elevation angles, used to define the orientation of the CS with respect to the anchor point. For illustration, the siphon is represented here as a straight line.

The siphon is initialized by arranging the LS and DS buckets starting from the anchor point and following a straight line, parallel to the segment OA, with the first bucket coincident with the anchor point. The velocity of the buckets at the beginning of the simulation is set to zero. In each simulation, the tether stiffness and damping are $EA = 21\,100\,\mathrm{N}$, $C = 2500\,\mathrm{N\,s}$ (values taken from Reference 15), while $k = 300\,\mathrm{N/m}$ and $c = 200\,\mathrm{Ns/m}$.

The siphon orientation is measured with respect to the CS (in general the chain shape will deform in the three dimensional space), using the local azimuth and elevation defined as in Fig. 5. Note that the elevation is defined with respect to the the plane passing through the anchor point and normal to the spin axis.

In all the simulations the asteroid mass is considered constant and effects of long-term mass removal are not taken into account, since the mass fraction removed is small.

RESULTS

Scenario 1. Figure 6 shows the CS azimuth, CS elevation, average anchor velocity (this is defined as $(1/n)\sum_{i=1}^{n}|\dot{\mathbf{r}}_i|$) and the z coordinate of bucket #1 for a $28\,\mathrm{h}$ simulation, for each case considered. The Coriolis forces due to the chain motion initially cause a counter-clockwise rotation of the chain (opposite to the asteroid rotation) and the amplitude of such oscillation is eventually reduced over time (Fig. 6a). A similar trend can be observed for the CS elevation (Fig. 6b). The variation of the CS elevation is due to the irregularities of the gravitational field, especially in close proximity to the asteroid, where buckets are deflected in the z direction (see also Fig. 6d) and the consequent oscillation is propagated to the other buckets of the chain and eventually to the CS.

The average chain velocity (Fig. 6c) reaches a steady value after an initial transient. The radial deceleration is due to payload refilling and is similar to the effect described in References 7 and 8: when a new payload mass is added at the bottom of the siphon, this mass is accelerated by the bucket while the average chain velocity decreases to conserve the linear momentum of the system. Hence, although the uppermost masses of the LS are generating a net radial force, the average chain velocity does not diverge, due to the deceleration phase caused by bucket refilling. Such a braking effect introduces elastic forces on the siphon, which are propagated along the entire chain. The higher frequency variations on the average chain velocity are a consequence of this effect.

Figure 7 is a view of the siphon from the positive z axis at the beginning of the fourth, fifth and sixth loop of the chain (the chain completes a *loop* when bucket #1 reaches the anchor after completing an entire ascent on the LS and descent on the DS) for the scenario (1a). The siphon is transversally streched, due to the opposite direction of the Coriolis forces on the two sides of the chain. In fact, the Coriolis forces induce a counter-clockwise rotation on the LS, and a clockwise rotation on the DS, due to the velocity of the buckets

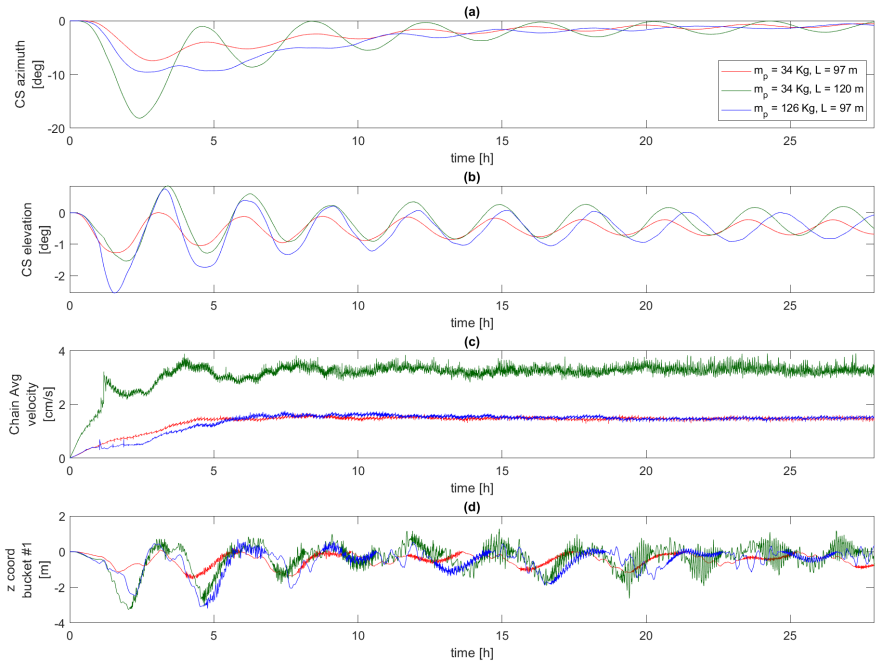

Figure 6: Scenario (1): CS azimuth, CS elevation and chain average velocity as a function of time (a) and coordinates of bucket #1 as a function of time (b).

being opposite on the two sides. The clockwise rotation induced by the DS contributes to reduce the CS azimuth over time.

Figure 8 shows the tension force on the tether connecting bucket #1 with bucket #2 during the third loop of the chain for all three cases. Overall, the tension force is very small, less than $0.2\,\mathrm{N}$ on average and with peaks below $2\,\mathrm{N}$ for scenarios (1b) and (1c). The peaks are associated with a new payload being attached to the bucket entering the LS. The amplitude of the peaks depends on the current configuration of the chain. In general, the tension force on the tethers increases for larger chain length or payload mass. This result is a requirement for a small anchoring force.

Scenario 2. Figure 9 shows the CS azimuth, CS elevation, average anchor velocity and the z coordinate of bucket #1 for a $50\,\mathrm{h}$ simulation, in the two cases considered.

Again, as in the previous scenario, the siphon rotates in the counterclockwise direction, opposite to the asteroid rotation, due to the Coriolis forces. After an initial transient, the CS azimuth is reduced and the chain tends to approach the local vertical (see also Fig. 10). It is interesting to observe that the variation of the CS elevation is rather small, although the asteroid shape is quite irregular. Therefore, it is expected that the centrifugal-induced forces on the uppermost payloads are large enough to counteract the z component of the gravitational acceleration on the lowermost masses. The equatorial displacement from the local vertical is much larger with respect to Scenario 1, due to the larger amount of mass on the LS, which introduces larger Coriolis forces. The difference between the cases (2a) and (2b) is not significant. The CS elevation in the case (2b) is slightly smaller in amplitude, due to the larger centrifugal-induced force available at the CS.

Figure 10 is a view of the siphon from the positive z axis at different timesteps for scenario 2a. The situation here is analogous to Fig. 7. In this case, the transversal stretching is larger at the beginning but it is

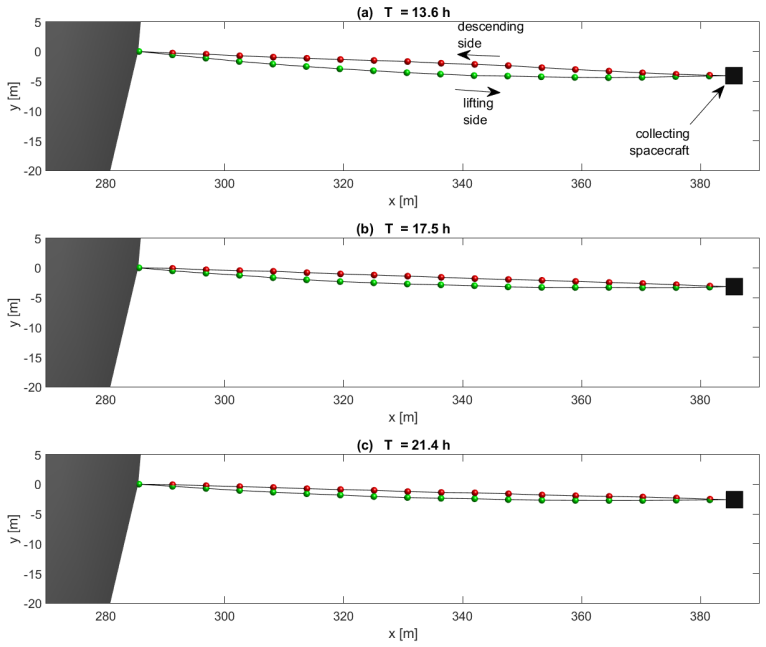

Figure 7: Scenario (1a): orbital siphon as viewed from the positive z axis.

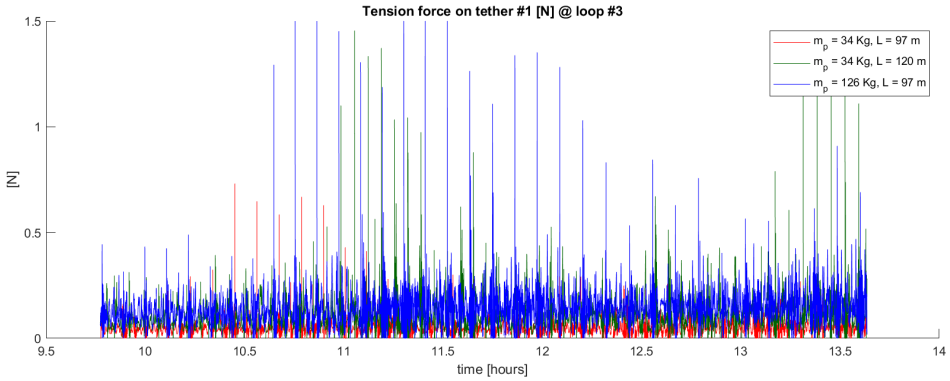

Figure 8: Tension force on the tether #1 during the third loop of the chain for the three cases in scenario 1.

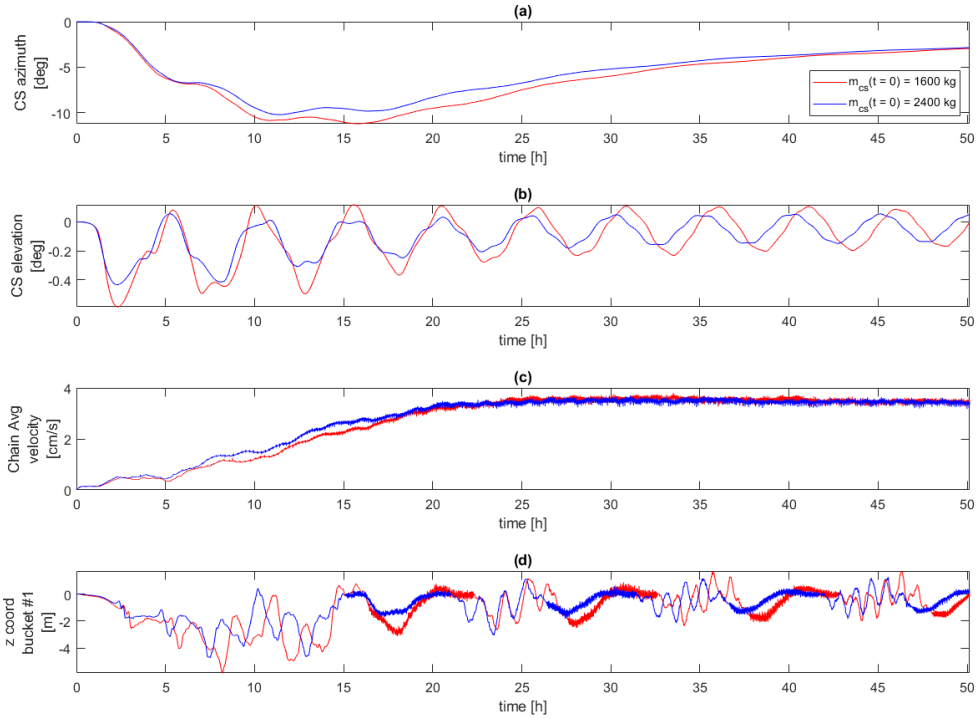

Figure 9: Scenario (2): CS azimuth, CS elevation and chain average velocity as a function of time (a) and coordinates of bucket #1 as a function of time (b).

reduced over time.

Scenario 3 - Siphon with moving base. Figure 11 shows the CS azimuth, CS elevation, average anchor velocity and the z coordinate of bucket #1 for a 58 h simulation of scenarios (3a) and (3b). The dotted vertical lines mark the interval when the siphon base is moving.

For the longitudinal base motion, the siphon changes its orientation to follow the direction of the centrifugal-induced force, which is parallel to the vector OA. The chain average velocity is larger during the base motion phase and then reduces once the base is fixed. The larger chain velocity is due to the additional centrifugal-induced acceleration caused by the moving anchor. The amplitude of the CS azimuth is reduced over time once the siphon base is fixed.

When the anchor is moving towards the positive z axis a significant change is noted in the CS elevation: the chain bends slightly southward (see Fig. 11b and Fig. 13). This effect is caused by the misalignment between the gravitational force and the centrifugal-induced force when the anchor moves northwards: the centrifugal-induced force on each bucket will keep the siphon perpendicular to the spin axis whereas the gravitational force is (approximately) pointing towards the asteroid center-of-mass, thus their sum has a net negative (positive if the siphon was moving southward) z component. This same effect has been noted in Reference 16, where the static behaviour of a non-equatorial space elevator was analysed for Earth application.

Figures 12 and 13 show the siphon at four different times during the simulation. Note from Fig. 12 that the siphon orientation adjusts during the anchor motion to follow the radial direction of the centrifugal-induced force. Moreover, for latitudinal motion, the bending effect is evident from Fig. 13.

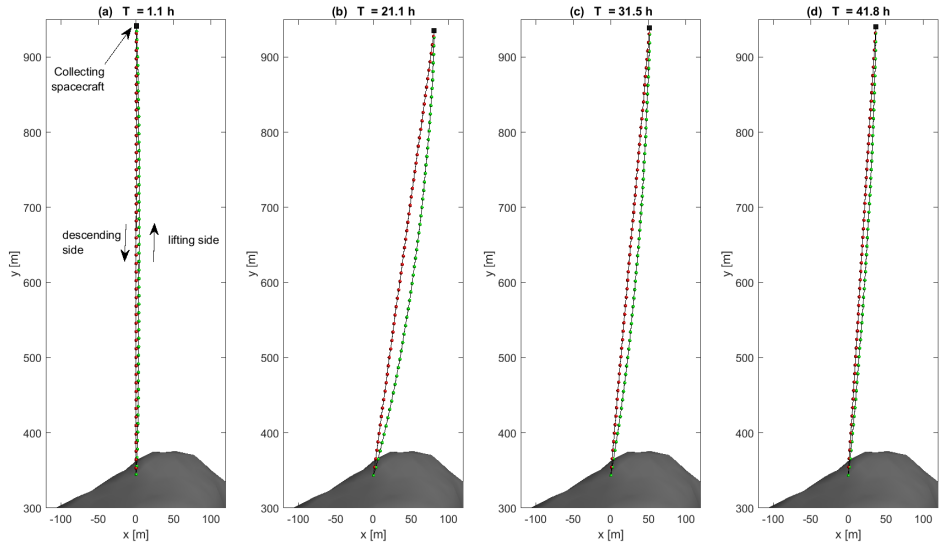

Figure 10: Scenario (2a): orbital siphon as viewed from the positive z axis.

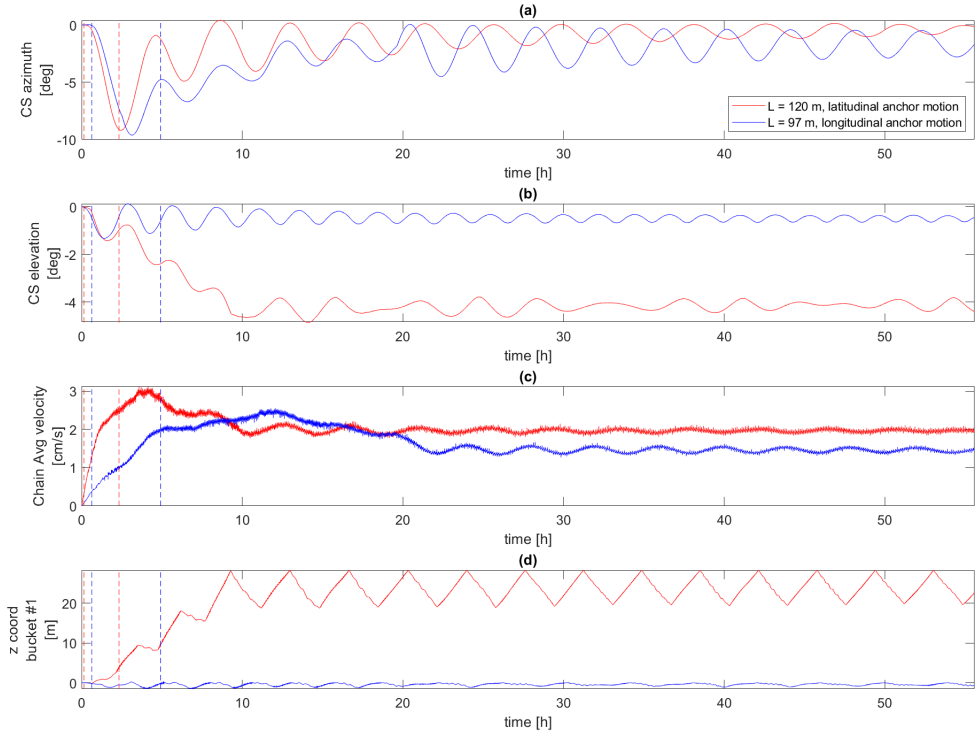

Figure 11: Scenario (3): CS azimuth, CS elevation and chain average velocity as a function of time. The dotted vertical lines mark the interval when the siphon base is moving.

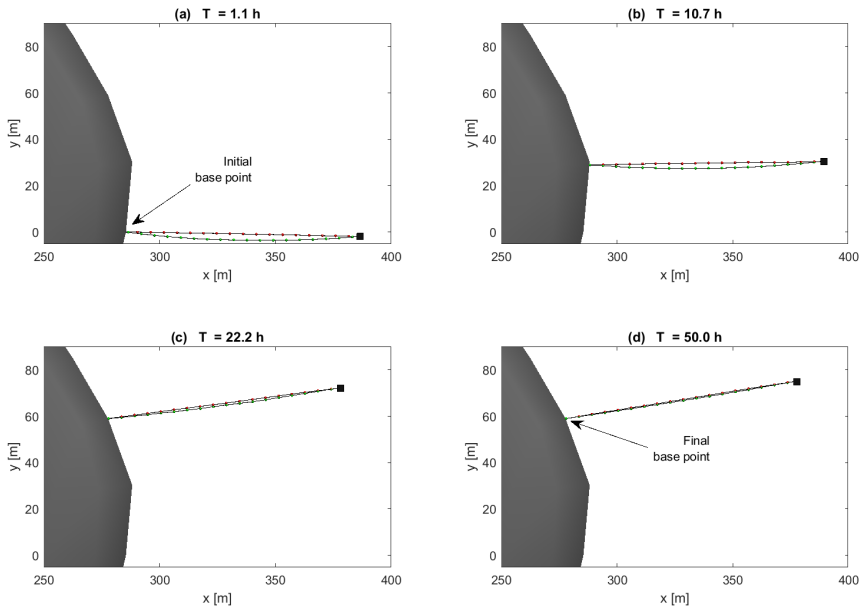

Figure 12: Scenario (3a): orbital siphon as viewed from the positive z axis.

DISCUSSION

Following the results, two key remarks can be made. First, the irregularities of the gravitational field do not introduce instabilities in the siphon dynamics. Some oscillations on the CS can be observed but their amplitude is reduced over time. Secondly, the siphon effect is generated using a self-sustaining tether-structure, without the payloads sliding on a rigid rod or a support tether. This is a key result: such a siphon architecture reduces the scale of infrastructure mass with respect to a siphon with support structure. Moreover, the lifting side and descending side of the siphon do not interfere or touch, due to the opposite direction of the Coriolis force on the two sides.

As in previous analyses[7,8], the average velocity of the chain for candidate asteroids is on the order of centimetres per second. Although seemingly small, the mass flow rate of material delivered to the CS can be increased by using larger payload masses. For example, using a $34\,\mathrm{kg}$ payload mass on Bennu the average mass flow rate is $288\,\mathrm{kg\,h^{-1}}$ (scenario (1a)), whereas for a $126\,\mathrm{kg}$ payload mass the mass flow rate raises to $1005\,\mathrm{kg\,h^{-1}}$ (scenario (1b)). One of the major disadvantages of large payload masses is the larger bucket volume required to host the material (in relation to the asteroid material density and porosity), which increases the structural mass of the siphon and hence the costs to deliver the infrastructure material to the asteroid. Other possible drawbacks of larger buckets are related to the bucket-cable attachment, and the sliding motion of the cable through the two pulleys in case of larger attachments. Further studies are required to investigate these engineering issues in detail.

By using longer siphons the average velocity of the chain increases, as the chain will benefit from larger centrifugal-induced force on the uppermost masses, thus in principle increasing the mass flow rate. However, it has been observed that the siphon length cannot arbitrarily increase. If the chain length increases, after a certain threshold (which depends on the asteroid, anchor location and tether properties) the radial velocity increases up to a point where the radial oscillation generated at each bucket refilling can destabilize the system, causing the chain to lose tension. This can be seen in part by comparing scenarios (1a) and (1c): in the case with a larger siphon length the chain average velocity oscillates with a larger amplitude and frequency. In particular, the non-equatorial oscillations in the z direction increase significantly (Fig. 6d). By further

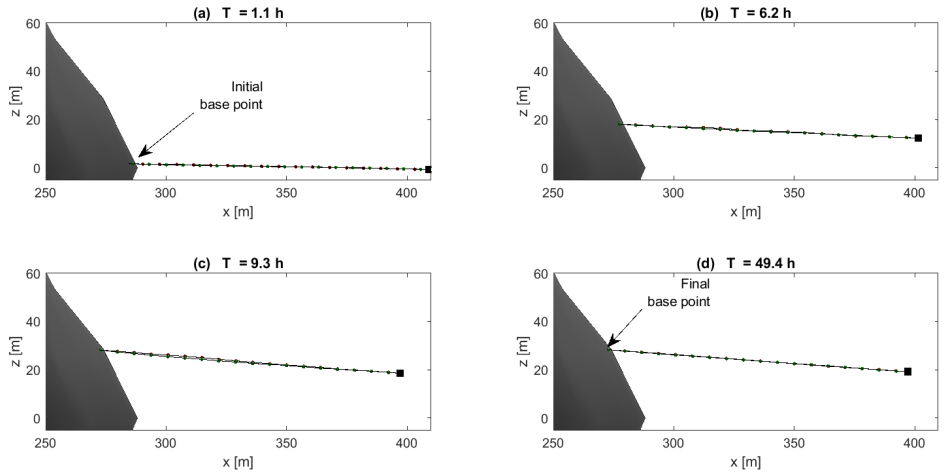

Figure 13: Scenario (3b): orbital siphon as viewed from the negative y axis.

increasing the siphon length to $130\,\mathrm{m}$ it is found that the siphon becomes unstable. This problem might be circumvented by dissipating residual oscillation through dampers located in proximity to the anchor and the CS. However, a siphon with a rigid support structure would not experience this issue, as any oscillation in a direction perpendicular to the structure would be damped by the structure itself, without propagating through the chain.

For the chain velocities considered here, the tension on the tethers is of the order of $1\,\mathrm{N}$. The small magnitude of the tension force is a consequence of the small length-scale of the structure involved, when compared to similar concepts applied at larger scales such as the *space elevator* for terrestrial applications.

The required anchor forces have the same order of magnitude as the tether forces. According to recent work on anchor mechanisms for asteroid landing and mining operations, it is possible to withstand much larger forces. For example, *area-of-effect softbots*[3] are soft-robotic spacecrafts with a large and flexible surface area to exploit the dynamical environment at rubble pile asteroids: a $1\,\mathrm{m}^2$ softbot can rely on a $10\,\mathrm{N}$ net force to remain anchored to the asteroid surface[3]. Other recent research on asteroid landing[17] compares the behaviour of different anchor tips in different media, claiming anchor forces between $36\,\mathrm{N}$ and $178\,\mathrm{N}$.

The dynamics of a siphon with a moving base was also investigated. In particular, the behaviour of a siphon undergoing small longitudinal and latitudinal anchor displacement on the surface of the asteroid Bennu has been analyzed. For a small base velocity ($1 \times 10^{-3}\,\mathrm{m\,s^{-1}}$) a siphon undergoing longitudinal motion tends to remain parallel to the radial direction defined by the centrifugal-induced force. Latitudinal surface motion causes a significant change of the CS elevation (Fig. 13), due to the misalignment between the gravitational force and the centrifugal-induced force. In both cases, the siphon has to be long enough to generate the orbital siphon effect at the desired final anchor location.

A siphon with a moving base may be a convenient solution to move the entire infrastructure to a different mining location without interrupting the delivery of material to the CS. However, this scenario calls for several engineering challenges. Among them is the efficient locomotion of the base on the asteroid surface, which is clearly influenced by small-scale surface features, e.g., boulders or cavities. An interesting solution is the recent *grappler* concept proposed in Reference 18. The key idea is to create a net-like mechanism by connecting multiple bi-stable array elements (called grapplers) that would grip variable asteroid terrain. In this case, the siphon base would move along a tethered structure defined by multiple grapplers adhering to the asteroid surface. The small siphon anchoring force requirements make the grapplers a viable solution to address the problem of a siphon with moving base.

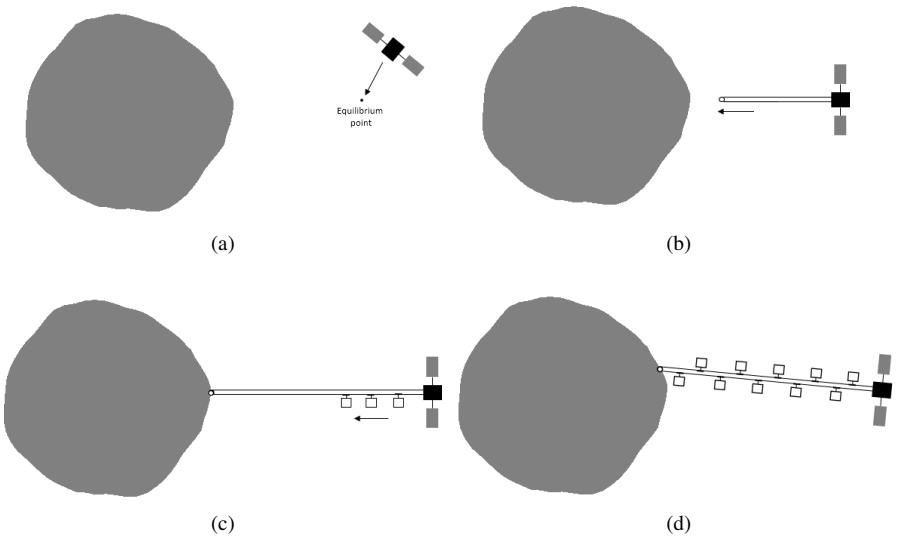

Figure 14: Concept of system deployment. (a) The CS approaches one of the asteroid equilibrium points. (b) The tether system is released. A propulsion system at the bottom of the tether controls the descent trajectory. (c) The tether is anchored to the asteroid surface or to the grippler system (in this case, the net-like structure has previously landed). The CS altitude is increased to reach the desired siphon length. Buckets are attached to the tether by cycling the tether using external torque applied to the pulleys. In this phase, the siphon structure can be exploited to land mining equipment (e.g., mining rovers) onto the surface. (d) The LS of the siphon is filled with material (again, external torque is required in this phase). When all the LS buckets are filled with payloads, the orbital siphon effect is initialized and the anchor base is translated to the desired location.

The power requirements to perform locomotion manoeuvrers on the surface will depend in general on the projection of the anchor force on the anchor velocity direction, on the magnitude of the anchor velocity and any friction involved. Neglecting friction, an anchor force of $1\,\mathrm{N}$ * in the direction of motion requires $1 \times 10^{-3}\,\mathrm{W}$ to move the siphon at a speed of $1 \times 10^{-3}\,\mathrm{m\,s^{-1}}$.

Deployment, operation and braking

Another significant engineering challenge is the deployment of the orbital siphon system. A proposed deployment scenario is to station the CS in proximity of an equilibrium point around the asteroid and then deploy the tether to the surface (see Fig. 14). To avoid deflection caused by inertial forces during the tether deployment, motion control is required in this phase, for example by using a propulsion system attached at the bottom of the tether. If a net-like structure is to be used to control the locomotion of the siphon base on the asteroid surface, this has to be landed in advance: the siphon anchoring device would then be attached to the gripller system. Once the anchor is fixed, the CS is raised to reach the desired siphon length.

Before attaching the buckets, the siphon tether can also be used as an elevator line to transfer mining rovers and the necessary mining equipment to the surface, including surface storage units, pre-processing units and power-supply units. Once the buckets are attached to the LS and DS of the tether, the siphon has to be initialized by filling the LS buckets with material. This phase requires an external input of energy: external torques can be applied to one of the two pulleys to rotate the chain, until all buckets on the LS are filled, after which the siphon will operate.

The nominal mass flow rate of the siphon is constrained by the technology available for the surface miners.

*Note that, in general, the component of the anchor force in the direction of anchor motion will be much smaller than the component normal to the asteroid surface.

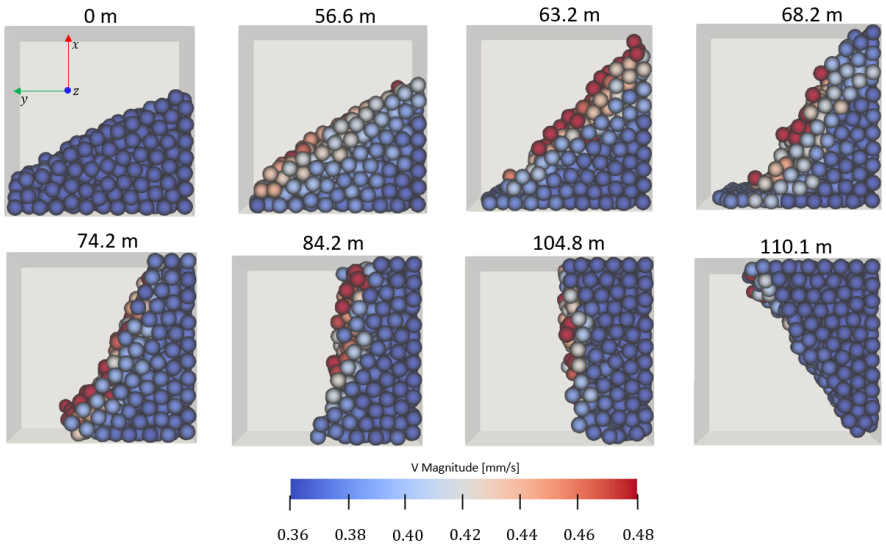

Figure 15: Motion of granular material inside a cubical bucket ascending a $120\,\mathrm{m}$ siphon anchored on Bennu. The altitude of the bucket is indicated in each figure.

These would transfer material to the siphon base for bucket refilling. The ability to extract large quantities of regolith with a large number of surface miners clearly increases the mass flow rate of material that can be delivered to the CS.

Granular dynamics

The simulation performed in this work has used a lumped mass model for the payload mass and the bucket. However, asteroid regolith is composed of particles with sizes in the millimetre to centimetre regime[19]. Knowledge of the granular dynamics inside the bucket and at bucket release is useful both to design an efficient material release system and to prevent material loss at the CS. Even though a thorough analysis of this problem is outside the scope of this paper, a brief discussion on the possible methods to address this problem is provided.

The Discrete Element Method (DEM) is a powerful tool to study the motion of a large number of particles under a given set of constraints and can be exploited to analyse the behaviour of granular material inside the buckets during the ascent on the LS and during release on the CS. For example, Figure 15 shows the dynamics of 662 spherical grains with $2\,\mathrm{cm}$ radius inside a cubical bucket with size $30\,\mathrm{cm}$ (Fig. 15). The simulation is performed considering the ascent of a partially filled bucket on the LS of a $120\,\mathrm{m}$ siphon anchored on Bennu, using a simplified spherical asteroid model and constraining the CS azimuth and elevation to remain zero (so the siphon is aligned with the x axis). In Fig. 15 the bucket is viewed from the positive z axis, with the positive x axis pointing towards the top of the page. The Coriolis acceleration is therefore pointing to the right (negative y direction). Regolith properties (Young Modulus, Poisson's ratio, coefficient of restitution and coefficient of friction) are taken from Reference 20.

Initially, the granular material experiences larger gravitational force and it accumulates on the side of the bucket closer to the asteroid. The Coriolis force causes the material to migrate towards the negative y axis. As the bucket altitude increases, the gravitational force reduces and the centripetal-induced force gradually increases. Material then starts migrating towards the positive x axis with small velocities below $0.5\,\mathrm{mm\,s^{-1}}$, accumulating on the upper-right of the bucket. Note that this transition occurs when the the bucket is approaching the synchronous orbit altitude, which for a spherical asteroid model is $69.8\,\mathrm{m}$ for Bennu. In order to improve the orbital siphon model, interaction between the bucket and the granular material inside it should be included in future analysis.

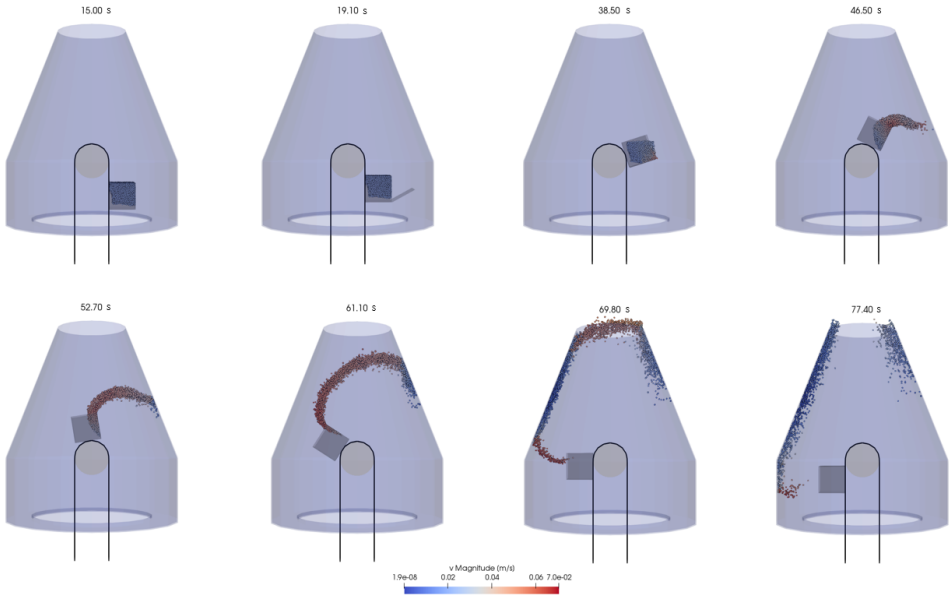

Figure 16: Release of material on the CS collector.

The centrifugal-induced force generated by the rotation of the bucket on the upper pulley can be exploited to transfer the payload material to the CS. Figure 16 shows the proposed concept for material removal. A conical hopper attached to the CS is envisaged to collect the material once released by each bucket. The centrifugal-induced force acting at the CS altitude will then cause material migration towards the convergent end of the hopper, after material is released. In this simulation the hatch is opened before approaching the pulley. This calls for an external trigger (electrical or mechanical) to activate and control the opening sequence. Another solution would be to exploit the acceleration induced by the rotation on the pulley to automatically open the hatch. A spring mechanism can be tuned such that during the ascent the hatch remain closed and it opens when the bucket rotates on the pulley.

CONCLUSION

In this paper, the dynamics of an orbital siphon anchored to a non-spherical asteroid has been investigated. The key idea behind the orbital siphon is that a chain of tether-connected masses arranged from the surface of a rotating asteroid can overcome the surface gravity of a rotating body and lift payload masses without the need for external work to be done. By releasing the upper payloads of the chain and adding new payloads at the bottom, an orbital siphon mechanism is initialized and a stream of masses can be delivered from the surface of the body into orbit or to a collecting spacecraft.

Expanding previous publications, here the siphon was not constrained to follow a radial path as no support structure was envisaged. Moreover, the material is released to on orbiting collecting spacecraft connected to the siphon which also serves as a counterweight to keep the system in tension. The two near-Earth asteroids 101955 Bennu and 6489 Golevka have been selected with the gravitational environment modelled using triangular-faced polyhedron models.

It has been shown that the orbital siphon effect is still generated under the hypotheses outlined. This is a key result, as the proposed siphon architecture reduces the scale of infrastructure mass with respect to a supported siphon. Moreover, the irregularities of the gravitational field do not introduce instabilities to the orbital siphon system or irregularly bend the chain. As in previous studies, the siphon radial velocity does not diverge but reaches a steady state, due to the constant deceleration accompanying each bucket refilling.

The dynamics of a siphon with moving anchor base has also been considered. It has been shown that the

siphon effect is still generated. This would allow the mining location to be moved without interrupting the flow of material to the CS.

ACKNOWLEDGEMENTS

CM is supported by a Royal Academy of Engineering Chair in Engineering Technologies and a Royal Society Wolfson Research Merit Award.

REFERENCES

[1] J. P. Sánchez Cuartielles and C. R. McInnes, "Assessment on the feasibility of future shepherding of asteroid resources," *Acta Astronautica*, Vol. 73, 2012, pp. 49–66.

[2] C. L. Gerlach, "Profitably Exploiting Near-Earth Object Resources," *Proceedings of the 2005 International Space Development Conference, National Space Society, Washington DC.*, 2005.

[3] J. McMahon, S. K. Mitchell, K. Oguri, N. Kellaris, D. Kuettel, C. Keplinger, and B. Bercovici, "Area-of-Effect Softbots (AoES) for Asteroid Proximity Operations," *2019 IEEE Aerospace Conference*, pp. 1–16.

[4] D. García Yárnoz, J. P. Sánchez Cuartielles, and C. R. McInnes, "Passive Sorting of Asteroid Material Using Solar Radiation Pressure," *Journal of Guidance, Control, and Dynamics*, Vol. 37, No. 4, 2014, pp. 1223–1235.

[5] C. R. McInnes, "Dynamics of a Particle Moving Along an Orbital Tower," *Journal of Guidance, Control, and Dynamics*, Vol. 28, No. 2, 2005, pp. 380–382.

[6] C. R. McInnes and C. Davis, "Novel payload dynamics on space elevators systems," *56th International Astronautical Congress. Fukuoka. 2005. IAC-05-D4.2.07*.

[7] A. Viale, C. R. McInnes, and M. Ceriotti, "Analytical mechanics of asteroid disassembly using the Orbital Siphon effect," *Proceedings of the Royal Society A: Mathematical, Physical and Engineering Sciences*, Vol. 474, No. 2220.

[8] A. Viale, C. R. McInnes, and M. Ceriotti, "Disassembly of Near Earth Asteroids by Leveraging Rotational Self Energy," *69th International Astronautical Congress, IAC-18-D4.3-18*.

[9] R. A. Werner and D. J. Scheeres, "Exterior gravitation of a polyhedron derived and compared with harmonic and mascon gravitation representations of asteroid 4769 Castalia," *Celestial Mechanics and Dynamical Astronomy*, Vol. 65, No. 3, pp. 313–344.

[10] D. J. Scheeres, S. G. Hesar, S. Tardivel, M. Hirabayashi, D. Farnocchia, J. W. McMahon, S. R. Chesley, O. Barnouin, R. P. Binzel, W. F. Bottke, M. G. Daly, J. P. Emery, C. W. Hergenrother, D. S. Lauretta, J. R. Marshall, P. Michel, M. C. Nolan, and K. J. Walsh, "The geophysical environment of Bennu," *Icarus*, Vol. 276, 2016, pp. 116–140.

[11] R. S. Hudson, R. F. Jurgens, K. D. Rosema, J. D. Giorgini, R. Winkler, R. Rose, D. Choate, R. A. Cormier, C. R. Franck, R. E. Frye, D. E. Howard, D. Kelley, R. W. Littlefair, M. A. Slade, L. A. M. Benner, M. L. Thomas, D. L. Mitchell, and P. W. Chodas, "Golevka Observations and Modeling 1 of 55 Radar Observations and Physical Modeling of Asteroid 6489," *Icarus*, 2000.

[12] S. R. Chesley, "Direct Detection of the Yarkovsky Effect by Radar Ranging to Asteroid 6489 Golevka," *Science*, Vol. 302, No. 5651, 2003, pp. 1739–1742.

[13] M. C. Nolan, C. Magri, E. S. Howell, L. A. M. Benner, J. D. Giorgini, C. W. Hergenrother, R. S. Hudson, D. S. Lauretta, J.-L. Margot, S. J. Ostro, and D. J. Scheeres, "Shape model and surface properties of the OSIRIS-REx target Asteroid (101955) Bennu from radar and lightcurve observations," *Icarus*, Vol. 226, No. 1, 2013, pp. 629–640.

[14] S. Mottola, A. Erikson, A. W. Harris, G. Hahn, G. Neukum, M. W. Buie, W. D. Sears, A. W. Harris, D. J. Tholen, and R. J. Whiteley, "Physical model of near-earth asteroid 6489 Golevka (1991 JX) from optical and infrared observations.," *The Astronomical Journal*, Vol. 114, 1997, p. 1234.

[15] J. Zhang, K. Yang, and R. Qi, "Dynamics and offset control of tethered space-tug system," *Acta Astronautica*, Vol. 142, 2018, pp. 232–252.

[16] B. Gassendy, "Non-Equatorial Uniform-Stress Space Elevators," *Proc. 3rd ISEC*, 2004.

[17] Z. Zhao, S. Wang, D. Li, H. Wang, Y. Wang, and J. Zhao, "Development of an Anchoring System for the Soft Asteroid Landing Exploration," *International Journal of Aerospace Engineering*, 2019.

[18] J. Cherston, P. Strohmeier, and J. A. Paradiso, "Grappler: Array of Bistable Elements For Pinching Net-Like Infrastructure to Low Gravity Bodies," *AIAA Scitech 2019 Forum*, 2019.

[19] B. Gundlach and J. Blum, "A new method to determine the grain size of planetary regolith," *Icarus*, Vol. 223, No. 1, 2013, pp. 479–492.

[20] Kulchitsky Anton V., Johnson Jerome B., Reeves David, and Wilkinson Allen, "Discrete Element Method Simulation of a Boulder Extraction from an Asteroid," *Earth and Space 2014*, pp. 485–494.